

ICRF-INDUCED DD FUSION PRODUCT LOSSES IN TFTR

D.S. DARROW, C.-S. CHANG*, S.J. ZWEBEN, R.V. BUDNY, H.W. HERRMANN,
E.F. JAEGER**, R. MAJESKI, M. MURAKAMI**, C.K. PHILLIPS, J.H. ROGERS,
G. SCHILLING, J.E. STEVENS[†], J.R. WILSON
Princeton Plasma Physics Laboratory,
Princeton University,
Princeton, New York, N.Y., United States of America

ABSTRACT. When ICRF power is applied to TFTR plasmas in which there is no externally supplied minority species, an enhanced loss of DD fusion products results. The loss occurs at the passing/trapped boundary, and consists of particles at or near their birth energy. The process appears to be the addition of perpendicular velocity to the fusion products as they interact with the ICRF waves, so that marginally passing particles are moved across the passing/trapped boundary into the first orbit loss cone. A simplified model of this process predicts losses of a magnitude similar to those seen. Extrapolations based upon these data for hypothetical ICRF ash removal from reactor plasmas suggest that the technique will not be energy efficient for removing fast alphas from the core.

1. INTRODUCTION

In numerous tokamaks ICRF heating has been used to heat the plasma and to increase its fusion reactivity. In some such scenarios, the ICRF waves act to accelerate minority species ions from the cold 'bulk' of the distribution. Other fast ions can also interact with the ICRF waves and absorb energy. In particular, fusion products (3 MeV protons, 1 MeV tritons and 0.8 MeV ^3He ions in DD plasmas, and 3.5 MeV alpha particles in DT plasmas) can absorb ICRF energy under some conditions [1]. This absorption can have several implications. The first is that some of these fusion products might be expelled from the plasma; several methods have been proposed based upon this process for ash removal from reactor-grade plasmas [2, 3]. A second possible implication is that ICRF heating scenarios may have to be chosen with care to avoid excessive absorption by the fusion products [4].

In this paper, we present observations of the loss of DD fusion products due to ICRF heating in TFTR, report on some initial modelling of the losses, and draw some conclusions about prospects for ash removal and for heating configurations in reactors.

2. PLASMA PARAMETERS, ICRF HEATING AND DIAGNOSTICS

In TFTR deuterium plasmas, the most common ICRF heating experiments are done with small amounts of either hydrogen or ^3He as the resonant species [5]. However, for the experiments discussed herein, ICRF power was applied to deuterium plasmas with no externally introduced minority species. The principal purpose of these experiments was to heat electrons by means of the fast wave [6, 7]. The only resonant species then were the DD fusion products produced by neutral beam injection (NBI).

The plasmas studied had the following parameters: $R = 2.62$ m, $a = 0.99$ m, $I_p = 1.8$ MA, $B_T = 4.5$ T, $P_{\text{NBI}} = 22$ MW, $f_{\text{ICRF}} = 47$ MHz, $P_{\text{ICRF}} = 0\text{--}3$ MW, $n_e(0) = 5.5 \times 10^{19}$ m $^{-3}$, $T_e(0) = 9$ keV, $T_i(0) = 16$ keV and $S_{\text{neut}} = 2 \times 10^{16}$ n/s. All four antennas on TFTR applied ICRF power. Because of reflected power and low single-pass absorption, it was not possible to increase the ICRF power above the 3 MW quoted above, even though up to 12 MW may be applied to the plasma in other scenarios. These parameters place the ^3He fundamental and the second harmonic of tritium inboard of the mag-

* Courant Institute for Mathematical Sciences, New York University, New York, N.Y., United States of America.

** Oak Ridge National Laboratory, Oak Ridge, Tennessee, United States of America.

[†] *Present affiliation:* Sandia National Laboratory, Albuquerque, New Mexico, United States of America.

netic axis, at $R = 2.56$ m. Under these conditions, the deuterium majority resonance and the resonances of the principal impurities are well off-axis. However, the DD fusion products, because of their high velocities, can satisfy the resonance condition $\omega = \Omega_i - k_{\parallel}v_{\parallel}$ over a large portion of the plasma. Depending upon their v_{\parallel} , fusion produced protons can be resonant anywhere in the plasma. Likewise, fusion produced tritons can be resonant anywhere between $R = 2.29$ m and $R = 2.92$ m. Given the fusion rate and the slowing down times of the DD fusion products, the maximum central concentration of 1 MeV tritons is very low, roughly $1.5 \times 10^{15} \text{ m}^{-3}$, and that of 3 MeV protons is about $5 \times 10^{14} \text{ m}^{-3}$, i.e. $n_{\text{fast}}/n_e \sim 10^{-5}$.

Measurements of the fusion product loss that results from the ICRF were made with the escaping fusion product diagnostic. This diagnostic consists of probes that can measure the pitch angle and gyroradius of escaping fusion products at four poloidal locations (at one toroidal angle) [8, 9], although the most interesting results are from the probe at 90° below the midplane. A schematic diagram of one of the probes is shown in Fig. 1, indicating how incident particles are dispersed according to pitch angle and gyroradius. Because the detector separates particles only by gyroradius and not by mass, it is not capable of distinguishing between the 3 MeV protons and the 1 MeV tritons produced by DD fusion reactions. In addition, a thin aluminium foil covers the inner aperture and

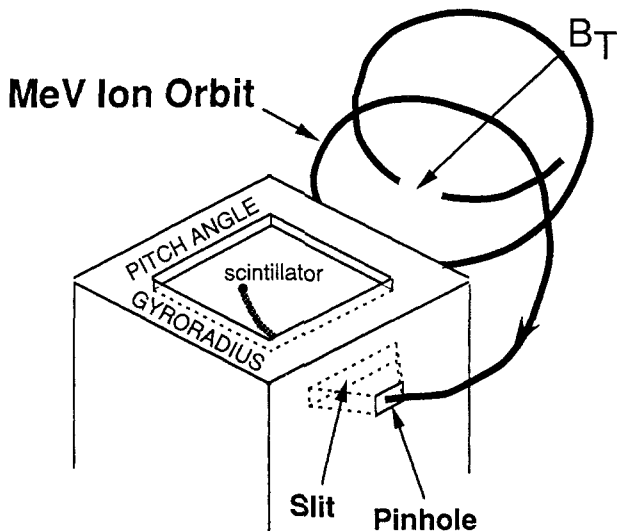


FIG. 1. Schematic view of one of the escaping fusion product probes on TFTR. Large gyroradius ions are able to enter the probe through two apertures spaced 1 cm apart. The arrangement of the apertures disperses the ions in gyroradius and pitch angle across the scintillator plate. A lens and fibre optic bundle in the probe stem carry the light from the scintillator to detectors away from the tokamak.

excludes hydrogenic ions with energies below 300 keV and helium ions with energies below 900 keV. The ions that are able to pass through the foil strike a scintillator plate and produce visible light. The image of light produced in the scintillator is carried by a fibre optic bundle to detectors in the basement of the TFTR facility. The detectors include photomultiplier tubes, which measure the total light produced in each probe, and an intensified videocamera, which records the light pattern on the scintillator. The pattern of light on the scintillators is then analysed to determine the gyroradii and pitch angles of the particles entering the detectors. Because the diagnostic signal-handling elements near the tokamak are purely optical, this system has very good immunity to radiofrequency produced noise, and no such noise was observed in these experiments.

3. EXPERIMENTAL RESULTS

A number of plasmas were produced with the parameters noted in the preceding section. In some discharges, the ICRF power was steady, while in others, it was modulated at 5 Hz. Figure 2 shows the ICRF and neutral beam powers, neutron rate and signals from three of the escaping fusion product detectors versus time for a discharge in which the ICRF power was modulated. This discharge had no significant MHD-induced fusion product loss. In discharges without substantial MHD or ICRF, the signals from the escaping fusion product probes vary in proportion to the neutron rate. This is because the predominant loss mechanisms of fusion products, first orbit loss and stochastic toroidal field ripple loss cause a fixed fraction of the production rate to escape when plasma conditions (especially plasma current) are not changing in time. In Fig. 2, there is a clear departure from that proportionality whenever the ICRF power is on, as evidenced by the synchronous enhancement of the loss signal on the 90° detector. There is also an ICRF related loss visible in the 45° detector data. This effect is barely discernible on the 60° detector for this and other discharges.

Figure 3 shows the fusion product loss rate at the 90° detector versus time divided by the total neutron rate, for the same shot shown in Fig. 2. Also shown is the ICRF power versus time, and the time during which the neutral beams are on. When plotted in this way, the effect of the ICRF is more apparent. In this shot, the application of 1.8 MW of ICRF power increases the normalized loss rate by $\sim 25\%$. The ICRF related loss is seen to turn on and off very quickly with the ICRF power, requiring ~ 5 ms to reach a steady value after turn-on, and

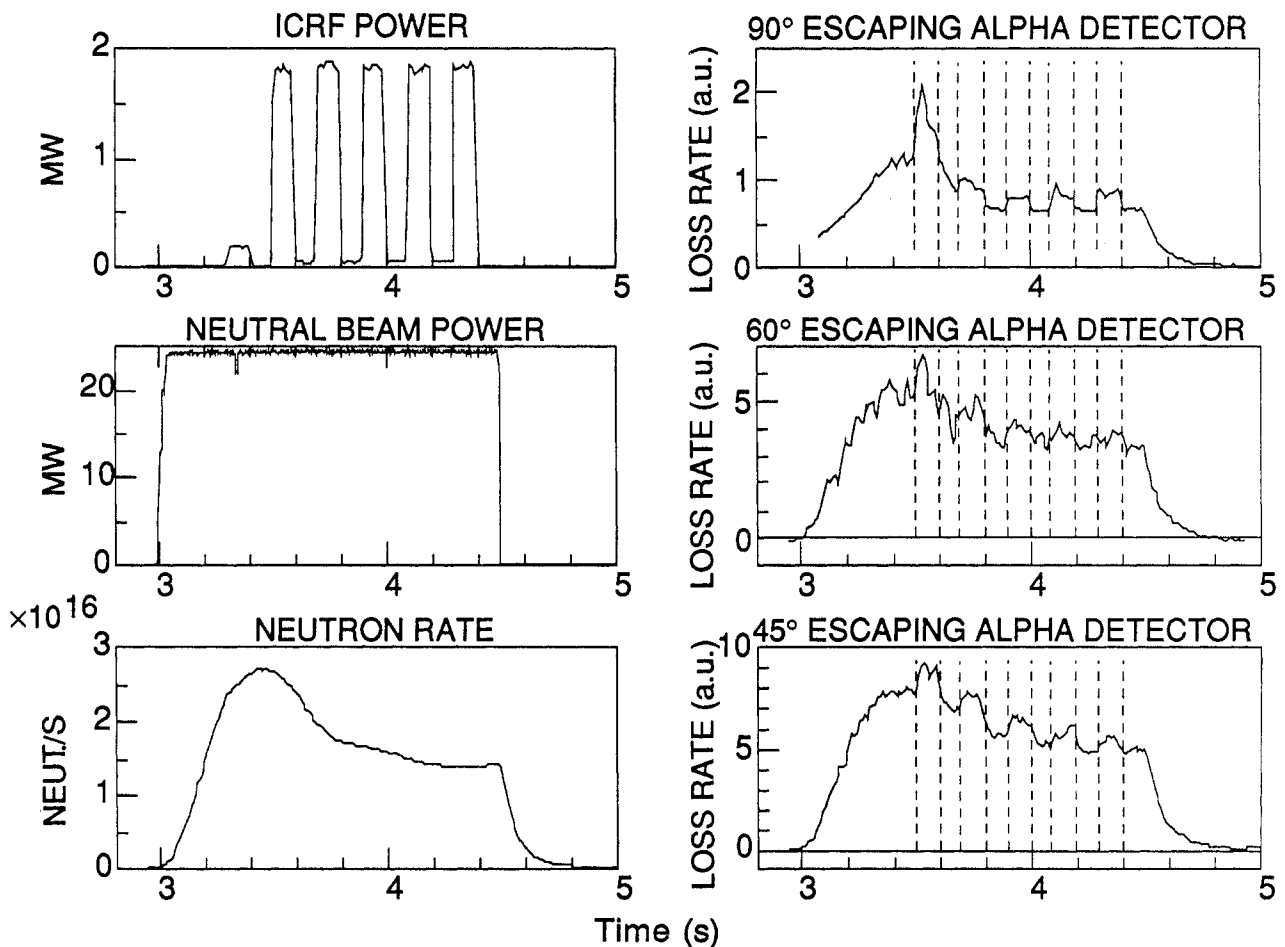


FIG. 2. Time histories of ICRF power, neutral beam power, neutron rate and rates of loss of fusion products to detectors at 90, 60 and 45° below the outer midplane. These traces are from TFTR shot 66 341, which had $I_p = 1.8$ MA, $R = 2.62$ m, $a = 0.99$ m, $B_T = 4.8$ T, $P_{NB} = 22$ MW, $P_{RF} = 1.8$ MW (5 Hz modulation) and $f_{RF} = 47$ MHz. The rates of fusion product loss on the 90 and 45° detectors follow the neutron rate, as expected, except for distinct increases synchronous with the ICRF pulses. There is no apparent modulation of the signal on the 60° detector during this discharge, although in other plasmas there is some sign of ICRF related loss there.

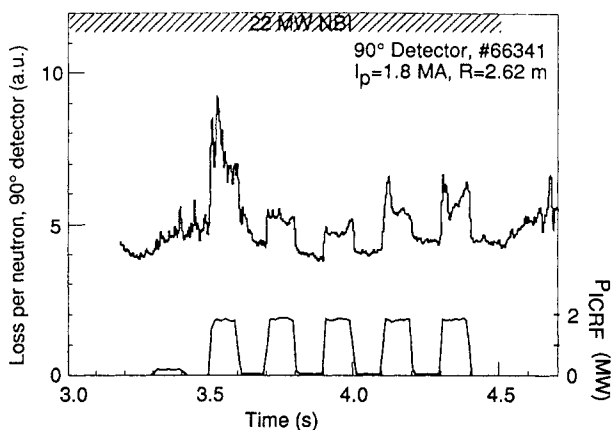


FIG. 3. Fusion product loss to the 90° detector, divided by the neutron rate, plotted versus time, along with the ICRF power. There is an enhancement of the loss synchronous with the ICRF power, which is about 25% above the baseline loss.

~ 1 ms to stabilize after turn-off. (The power is switched on and off in less than 0.5 ms.) These times are short compared with the 90° pitch angle scattering time for these fusion products, 17 s for protons and 11 s for tritons. There is a significant degree of variation in the loss rate during the times when the ICRF is on, but there is as yet no explanation for this variability, nor any observed correlation of these fluctuations with other signals from the plasma.

The data for Figs 2 and 3 are taken from photomultipliers that measure the total light coming from the scintillator of each probe. More detailed information about the pitch angle and gyroradius of the loss can be extracted from images of the scintillators taken by an intensified videocamera. Figure 4(a) presents plots of the light intensity, normalized to the neutron rate, versus gyroradius co-ordinate in the 90° detector, integrated

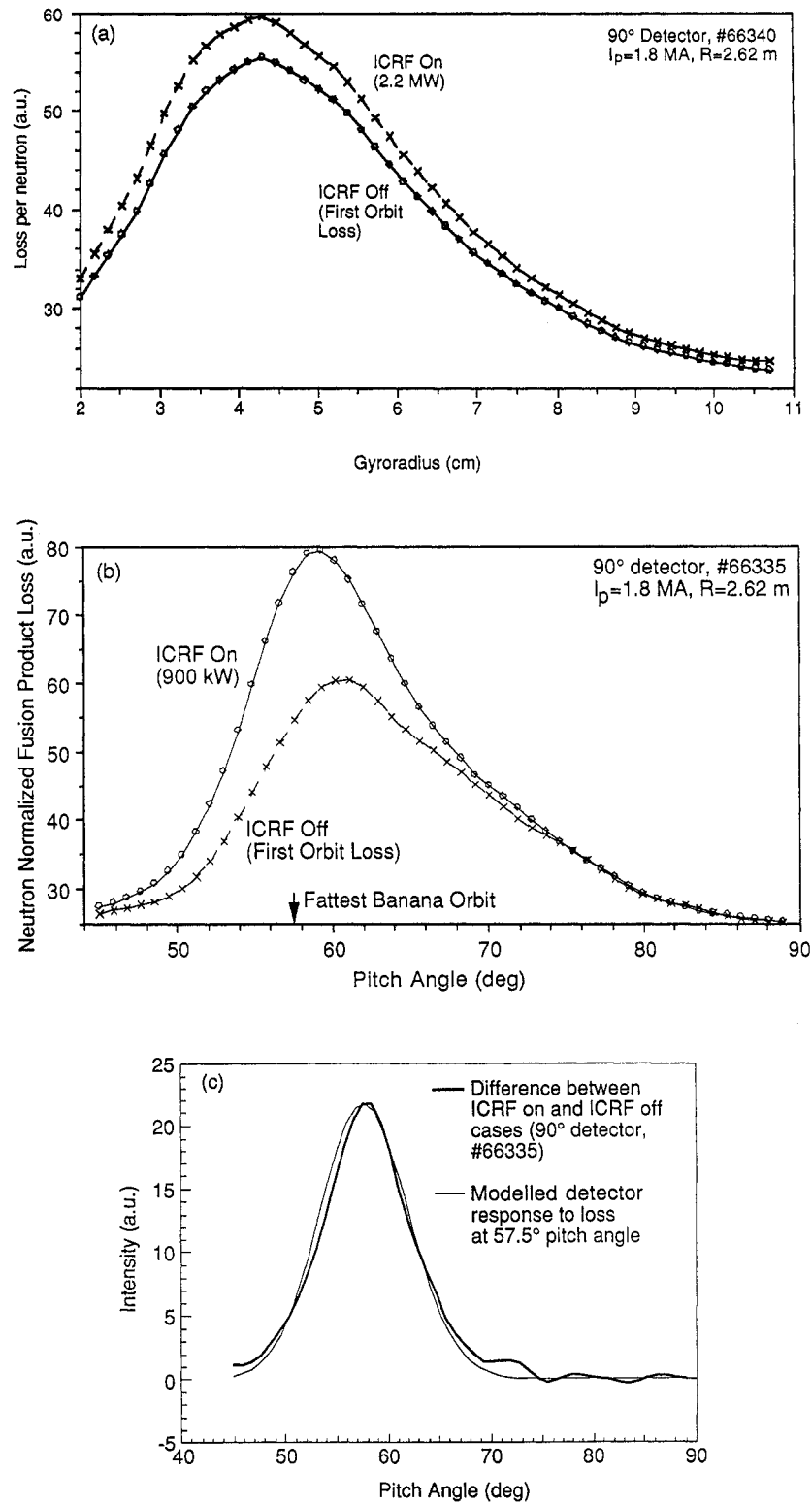


FIG. 4. (a) Comparison of the gyroradius distributions on the scintillator in the 90° probe with and without ICRF. (b) Comparison of the pitch angle distributions on the scintillator with and without ICRF. (c) The difference in the pitch angle distributions with and without ICRF compared with the modelled response of the detector to the pitch angle of the passing/trapped boundary. The loss at this pitch angle, with the instrumental broadening, is sufficient to explain the observed change in the pitch angle distribution.

over all pitch angles for two time intervals: with and without ICRF. The curve labelled 'ICRF off' in this figure comprises almost exclusively first orbit loss of fusion products at their birth energies. (DD fusion-produced protons and tritons have the same gyroradius at birth.) The width of the gyroradius distribution results entirely from the characteristics of the instrumental response. References [1] and [7] show the good agreement between measured gyroradius distributions like that seen in Fig. 4(a) and numerical modelling of the detector response to first orbit loss distributions. In Fig. 4(a), only the amplitude, and not the shape, of the gyroradius distribution changes when the ICRF is applied. Hence, the added loss during the ICRF power is inferred to be at the birth energy, within the energy resolution of the detector of about $\pm 20\%$.

Figure 4(b) compares the pitch angle distribution of the lost fusion products, integrated over all gyroradii and normalized to the neutron rate, for the same data as in Fig. 4(a). There is again some instrumental broadening of the distribution. Here, the loss at pitch angles above 67° is essentially unaffected by the application of ICRF. However, below 67° , there is a significant enhancement to the loss when the ICRF is applied. This enhancement is maximum at $\sim 57.5^\circ$ pitch angle, which coincides with the fattest banana orbit that enters this probe. The fattest banana orbit, of course, coincides with the boundary between trapped and passing orbits. The ICRF induced loss on the 60° and 45° probes also appears at the pitch angle of the fattest banana orbit.

The instrumental function is such that the observed change in the pitch angle distribution in the 90° probe is consistent with all the ICRF related loss coming at the fattest banana orbit. This is portrayed in Fig. 4(c), in which the difference between the two pitch angle distributions plotted in Fig. 4(b) is compared with a model of the probe's response. The model assumes a loss of particles only at the pitch angle of the passing/trapped boundary, 57.5° , and computes the output pitch angle distribution, incorporating the spreading due to the slit widths and the optical resolution of the probe system. The agreement between the two curves is quite close, indicating that the ICRF induced component of the loss occurs exclusively at the passing/trapped boundary. The pitch angle distribution in the case with no ICRF, shown in Fig. 4(b), corresponds to first orbit loss. It is broader than the ICRF induced loss because the lost particles are born over a range of pitch angles that lie within the loss cone.

Figure 5 depicts the scaling of the ICRF related enhancement factor, which is the increase in the normalized loss during ICRF divided by the normalized loss with no ICRF, versus the ICRF power for a number of shots

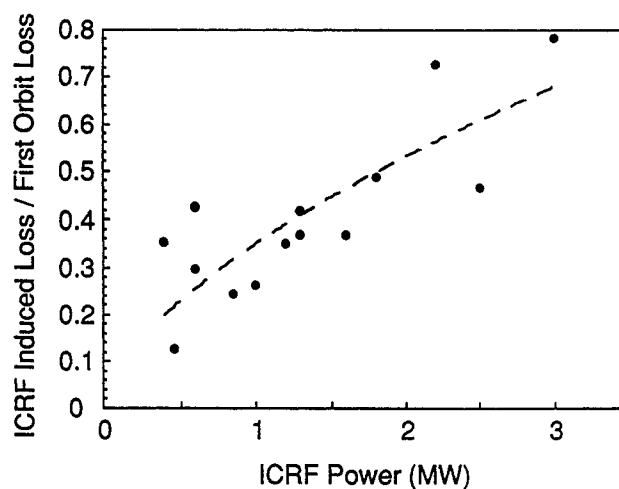


FIG. 5. Ratio of the ICRF enhanced loss to the first orbit loss as a function of ICRF power for 1.8 MA, $R = 2.62$ m discharges in TFTR. The dashed line is the best least squares fit to a power law form, $F_{RF} = AP_{RF}^\beta$, with the results $A = 0.35 \pm 0.03$ and $\beta = 0.61 \pm 0.14$.

in the range 66 317 to 66 342. There is a definite increase as the ICRF power is raised. At the highest ICRF powers used in this experiment, 3 MW, the loss of fusion products is enhanced by a factor of almost 1.8.

4. MODELLING OF THE LOSS

The salient characteristics of the ICRF-induced fusion product loss, derived from the experimental observations above, are these: the loss is at the passing/trapped boundary (fattest banana orbit) in the 90° detector, is near the birth energy of DD fusion products, and turns on and off much more rapidly than the collisional 90° pitch angle scattering times of the particles. Three possible ICRF-induced loss processes could produce these signatures:

- (a) Direct increase in the fusion products' perpendicular velocities by the ICRF, which carries barely passing particles into the first orbit loss cone at the fattest banana orbit [10];
- (b) ICRF-induced diffusion of barely passing particles outward in minor radius until they undergo magnetic mirroring at the high field side of their orbits, escaping onto the fattest banana orbits [11–15];
- (c) Spiralling outward in minor radius of barely passing particles due to asymmetric variation of their velocities as they encounter localized ICRF acceleration and collisional slowing down, the result being the same as in (b) [16].

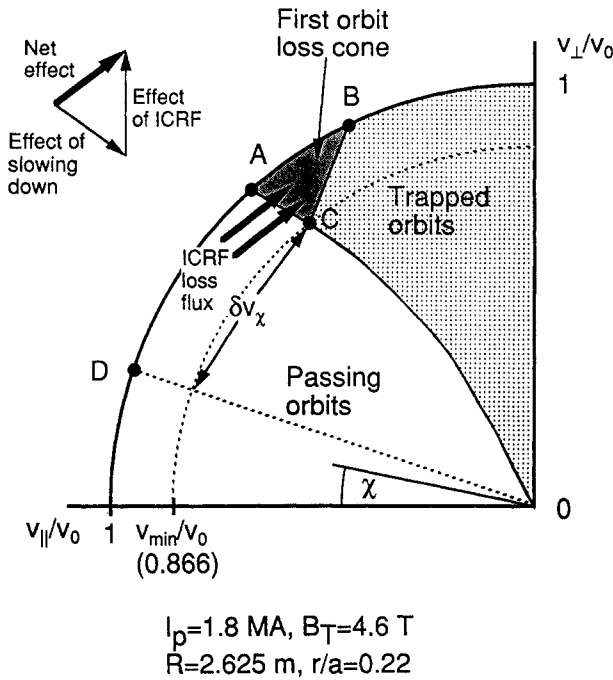


FIG. 6. Diagram of the postulated ICRF induced loss process. The effects are shown of collisional slowing down and ICRF acceleration of the fusion products. The net result is that some particles are carried into the loss cone. The rate of slowing down and the rate of ICRF heating determine the range of χ at birth that will be transported into the loss cone. The point at the limit of the range of χ that will be lost owing to ICRF is labelled D.

Of these, the first process is far faster, according to theory, than the others. Hence, only the first process was modelled and only this process is discussed in what follows.

Figure 6 shows schematically process (a) above in velocity space. This figure shows only the countergoing (i.e. opposite the direction of the plasma current) portion of velocity space. In addition, it applies only to the particular plasma current used in this experiment, $I_p = 1.8 \text{ MA}$, and only to a particular magnetic surface, the one at $r/a = 0.22$. This flux surface is chosen because it is the one that produces the largest first orbit loss signal in the 90° detector, since its marginally trapped fusion product orbits are just able to reach that detector. The figure applies to both 1 MeV tritons and 3 MeV protons, since their orbits are identical if they have the same pitch angle. The simplified model used here considers only the flux surface whose characteristics are depicted in Fig. 6. The triangular region is the first orbit loss cone. Note that there is a minimum total velocity below which all particles are confined at this minor radius. Fusion products, in this model, can be affected by two processes:

collisional slowing down and ICRF heating. Collisional pitch angle scattering is a much weaker effect than the scattering produced by ICRF heating and, hence, is neglected. Slowing down acts to move a particle directly towards the origin, while ICRF heating causes a vertical motion in Fig. 6. The combined effect of collisional slowing down and ICRF heating together is to carry barely passing particles into the loss cone. The stronger the effect of the ICRF compared with the slowing down rate, the larger will be the ICRF enhancement of the first orbit loss. Pitch angle scattering can also carry particles into the loss cone [17], but at a markedly smaller rate than the ICRF waves, as noted above.

The rate of pitch angle scattering due to the ICRF in a time δt can be approximated by [17]

$$\delta v_\chi = v_0 (\delta t \nu_{\text{RF}})^{1/2} \cos \chi \quad (1)$$

The effect of ICRF is represented as an effective collisionality, with $\nu_{\text{RF}} = 2p_{\text{abs}}/m_f n_f v_f^2$. Here, m_f is the fast ion mass, n_f is the fast ion density, v_f is the fast ion velocity, p_{abs} is the ICRF power density absorbed in the fast ions and ν_{RF} is the e-folding rate for the energy of the fast ions (neglecting Coulomb slowing down). The first part of the expression for $v_0(\delta t \nu_{\text{RF}})^{1/2}$ is the change in the particle's v_\perp due to the ICRF, from which the component acting to change the particle's pitch angle must be computed by multiplying by $\cos \chi$. For the conditions present in these discharges, the PICES code [18], which is a 3-D full wave code developed at ORNL, computes the power absorbed in the tritons, for the case $P_{\text{RF}} = 1.8 \text{ MW}$, to be $p_{\text{abs}} = 500 \text{ W/m}^3$. This absorption calculation assumes a central triton density, as computed

TABLE I. PARAMETERS OF FUSION-BORN TRITONS AND PROTONS

	1 MeV tritons	3 MeV protons
v_f (at birth) (m/s)	8.0×10^6	2.4×10^7
n_f (m^{-3})	1.5×10^{15}	5.0×10^{14}
p_{abs} (W/m^3)	500 (PICES result)	500 (assumed)
ν_{RF} (s^{-1})	2.0	2.0
v_{min} (m/s)	6.9×10^6	2.1×10^7
δt (s)	0.28	0.039
δv_χ (m/s)	4.0×10^6	4.5×10^6
$\delta \chi$ (deg)	33.0	12.3
F_{RF}	1.2	0.70

by the transport code TRANSP [19], of $1.5 \times 10^{15} \text{ m}^{-3}$ (about 2.8×10^{-5} of the central electron density), a radial profile of triton density that varies as $[1 - (r/a)^2]^8$ and a Maxwellian distribution function with a temperature of 600 keV, roughly approximating the slowing down distribution of the tritons. The distribution function in the experiment is non-Maxwellian, but the PICES code, at present, is unable to accommodate such distributions. Hence, the absorbed power figure above is only an estimate. The PICES code is not able to calculate the Doppler shifted absorption of the waves by 3 MeV protons, but another calculation [20] indicates that the power absorbed by them is equal to that absorbed by the tritons. From this, an estimate of their loss rate can also be obtained. The parameters of fusion-born tritons and protons, and the corresponding values of ν_{RF} , are given in Table I for $r/a = 0.22$.

On a given flux surface, there is a minimum velocity, ν_{min} , below which ions cannot enter the loss cone. A fast ion will be lost only if its pitch angle at birth is close enough to the passing/trapped boundary that it can be swept into the loss cone before slowing below ν_{min} . Hence, the time interval δt in Eq. (1) is the time for the fast ion to slow down from ν_0 to ν_{min} . δt is given, to first approximation, by the collisional slowing down time, although a more exact treatment would have to incorporate the effect of ICRF heating on δt also. The change in pitch angle due to the effect of ICRF over the given time δt is then $\delta\chi \approx \delta\nu_\chi/\nu_{\text{min}}$. The values of ν_{min} , δt and the resultant $\delta\nu_\chi$ and $\delta\chi$ are also reported in Table I. From $\delta\chi$ and the pitch angle associated with point C in Fig. 6, the pitch angle of point D can be calculated. D is the limiting point, beyond which the ICRF is unable to draw thermalizing fast ions into the loss cone. The coordinates of points A, B, C and D are listed in Table II.

Since the loss in the absence of the ICRF waves is first orbit loss, it is convenient to compare the magnitude of

the loss during ICRF to first orbit loss. The energy distributions of both losses indicate that near birth energy particles are being lost. Particles are born on the $\nu/\nu_0 = 1$ circle with a density proportional to $\sin\chi$. To compare the magnitude of the losses, compute the ratio of the birth rate along arc DA to that along arc AB,

$$F_{\text{RF}} = \frac{\int_D^A \sin\chi \, d\chi}{\int_A^B \sin\chi \, d\chi} = \frac{\cos\chi_D - \cos\chi_A}{\cos\chi_A - \cos\chi_B} \quad (2)$$

For 1 MeV tritons, this ratio is 1.2; for 3 MeV protons, it is 0.70. By way of comparison, the ratio of loss during ICRF to first orbit loss was only ~ 0.25 in the 1.8 MW case shown in Figs 2 to 4.

The detector is unable to discriminate between 3 MeV protons and 1 MeV tritons since it only disperses particles based upon their gyroradii. Owing to details of the response of the scintillators used in the detectors [21], about 70% of the first orbit loss signal is due to protons and the remaining 30% is due to tritons. If the proton loss rate alone increased by 70% as predicted above, the total signal to the detector should increase by 49%. If the triton loss rate alone rose by the predicted 120%, the total signal to the detector should increase by 36%. These total to an increase of 85%. This is significantly larger than the total observed increase in loss rate of only 25%. Particles of both species with pitch angles near the passing/trapped boundary can, for the conditions of this discharge, resonate with the ICRF waves. Hence, it seems probable that both species contribute to the enhancement of the loss.

Figure 5 shows the ratio F_{RF} versus applied ICRF power. The dashed line is the best least squares fit to a form $F_{\text{RF}} = AP_{\text{RF}}^\beta$, where A and β are constants. Assuming p_{abs} is linear in P_{RF} , and keeping only the leading order terms in a power expansion for Eq. (2), the exponent β should be 0.5. The result from least squares fitting is $\beta = 0.61 \pm 0.14$ for this dataset, agreeing, within uncertainties, with the model.

There are several shortcomings in the model used above, and these may explain the significant difference in magnitude between the experimental and model results. The model presented above considers only one magnetic surface, and only one orbit from that surface. A more precise and complete model would compute the actual flux of particles to the chosen detector from the range of flux surfaces and pitch angles that can be seen by that detector. Another shortcoming is that the ICRF power absorption in PICES can only be calculated with a Maxwellian distribution function, and not the slowing down distribution expected for fusion products. In addition, ν_{RF} is a func-

TABLE II. CO-ORDINATES OF POINTS A, B, C AND D

	ν/ν_0	χ (deg)	$\cos\chi$
A	1.0	48.5	0.66
B	1.0	64	0.44
C	0.866	52	0.62
D (for 1 MeV tritons)	1.0	19	0.95
D (for 3 MeV protons)	1.0	40	0.77

tion of a particle's energy and pitch angle, but that dependence has not been included here.

There is also an inconsistency between the experimental data and the model presented above. The experimental data indicate that, within the resolution of the detectors, the loss is coming out at the birth energy. In contrast, the model above predicts a distribution of energies between the birth energy and the energy corresponding to the lower edge of the loss cone. The lower edge of the loss cone is at $0.75E_{\text{birth}}$.

5. DISCUSSION

In the foregoing sections, it has been established that the observed characteristics of the ICRF related loss are consistent with this loss being due to an increase of the particles' v_{\perp} by ICRF, so that these particles are carried into the first orbit loss cone. In addition, there is rough quantitative agreement between the observed and modelled loss rates. Hence, we believe that the mechanism of the loss has been identified.

The mechanism proposed here also acts upon trapped particles. For certain classes of trapped particles, additional v_{\perp} causes their banana tips to move such that they become subject to stochastic toroidal field ripple loss [22, 23]. Hence, there should have been an increase in such ripple losses during these experiments. Unfortunately, none of the probes at 90, 60 or 45° below the midplane are situated where they should observe ripple loss. There is a movable detector at 20° below the midplane [24] that can detect ripple lost fusion products, but it was not in use during the experiments described in this paper, so no supporting experimental evidence for this hypothesis can be presented.

Reference [1] also presents measurements of fast ion losses from TFTR during ^3He minority ICRF heating. The plasmas described in this work contain neutral beam ions and DD fusion products. In contrast, the plasmas described in Ref. [1] contain neutral beam ions, DD fusion products, D^3He fusion products and ^3He tail ions. Since the detectors cannot discriminate the mass of the ions lost, the larger variety of fast ions tends to increase the number of possible interpretations of the measurements made. For instance, in the data presented here, the fusion product source rate is known from neutron measurements. In Ref. [1], though, the D^3He reaction rate is not known, since the reaction produces no neutrons, and so the only means of distinguishing ICRF-induced fusion product loss from first orbit loss is through their pitch angle distributions. Figure 5 in Ref. [1] indicates that the pitch angle distribution in the

90° detector changes very little when ICRF is added to NBI discharges, validating the interpretation given there that the added loss is due to D^3He reactions created by the ICRF heating.

Reference [1] also reports a factor of 10 increase in the loss to the 45° detector during the same plasmas. The reason for this could not be definitely established, but some of the signal was attributed to ICRF induced loss of fusion products, since the gyroradius of the loss was that of fusion products. There would also be the increased loss due to increased D^3He reactivity, as was seen in the 90° detector. In contrast, the ICRF induced loss at the 45° detector reported here in Fig. 2 is of a percentage similar to or smaller than that in the 90° detector, and *not* several times the first orbit loss level. An alternative explanation of the large ICRF induced losses to the 45° detector reported in Ref. [1] is that some of the ^3He tail ions are being lost to this detector. Losses of tail ions to this detector have been seen on numerous occasions. This hypothesis would also explain the elongation of the loss towards higher pitch angle, as these tail ion losses tend to occur at pitch angles significantly higher than the fusion product fastest banana pitch angle. A loss of less than 1% of the tail ion population could produce the signal seen. The loss of tail ions is also invoked as the explanation of the large increases in losses seen in the 45° detector during other ^3He minority ICRF heating experiments [25].

It is possible, from the results reported here, to draw some initial conclusions concerning possible applications of this ICRF induced loss. The first point to note is that the first orbit loss level is nearly doubled when 3 MW of ICRF is applied. The first orbit loss rate from a 1.8 MA shot in TFTR is $\sim 3\%$. This means that ICRF expulsion of fusion products can constitute $\sim 3\%$ of the source rate. (This is only an order of magnitude estimate, since the data in Fig. 2 show that the poloidal distribution of the ICRF induced loss is not the same as that of the baseline loss.) This loss mechanism depends upon the existence of a first orbit loss cone. For reactor-size devices, such as ITER, that loss cone will exist only near the edge. Hence, loss of alpha particles from the centre is likely to be negligible. This would seem to suggest that ICRF induced alpha loss of this type will not place significant constraints upon ICRF heating scenarios for large devices. Closer to the edge, though, the first orbit loss cone grows large, and so ICRF might be useful as an ash removal method.

There are some limitations to ash removal implied by these observations. First, the ICRF induced losses observed in this experiment were of fusion products at or near their birth energy. This means that the fusion products have given little or none of their energy to the plasma before being expelled, potentially reducing the

self-heating of the plasma and increasing the heat load on the first wall. Second, the energy efficiency of this process is low. About 2.4 kW of ICRF power is computed to have been absorbed by the fusion products, resulting in the loss of particles whose total fusion power is ~ 400 W, to within a factor of 2. (There is some inconsistency here, since if all that 2.4 kW was absorbed by the fusion products, their energies would be $\sim 20\%$ above their birth energies, something which should have been visible in the loss signals, but was not seen.)

Further work is planned in two broad areas relating to these losses. First, as mentioned above, quantitative numerical models are being formulated to model the flux to the detectors resulting from ICRF better. Second, an experiment to try several possible means of influencing alpha particles with ICRF has been proposed for TFTR's DT phase.

ACKNOWLEDGEMENTS

We wish to acknowledge the efforts of the TFTR Operations and ICRF groups for their technical support of this experiment. We also thank D. van Eester for his calculations of the rate of ICRF absorption by 3 MeV protons in these plasmas. This work was supported by USDOE contract No. DE-AC02-76-CHO-3073.

REFERENCES

- [1] ZWEBEN, S.J., et al., Nucl. Fusion **32** (1992) 1823.
- [2] TFR GROUP, Nucl. Fusion **22** (1982) 956.
- [3] COHEN, S.A., et al., Bull. Am. Phys. Soc. **37** (1992) 1396.
- [4] LAM, N.T., et al., Nucl. Fusion **34** (1994) 1161.
- [5] TAYLOR, G., et al., Plasma Phys. Control. Fusion **36** (1994) 523.
- [6] MURAKAMI, M., et al., in Radio Frequency Power in Plasmas (Proc. 10th Top. Conf. Boston, 1993), AIP, New York (1994) 48.
- [7] MURAKAMI, M., et al., in Controlled Fusion and Plasma Physics (Proc. 20th Eur. Conf. Lisbon, 1993), Vol. 17C, Part III, European Physical Society, Geneva (1993) 981.
- [8] ZWEBEN, S.J., et al., Nucl. Fusion **30** (1990) 1551.
- [9] ZWEBEN, S.J., et al., Nucl. Fusion **33** (1993) 705.
- [10] CHANG, C.S., Phys. Fluids **28** (1985) 3598.
- [11] CHEN, L., et al., Nucl. Fusion **28** (1988) 389.
- [12] YAMAGIWA, M., Phys. Plasmas **1** (1994) 205.
- [13] CORE, W.G.F., Nucl. Fusion **29** (1989) 1101.
- [14] HELLSTEN, T., Plasma Phys. Control. Fusion **31** (1989) 1391.
- [15] KOVANEN, M.A., et al., Nucl. Fusion **32** (1992) 787.
- [16] CHANG, C.S., et al., Phys. Fluids B **3** (1991) 3429; FINKEN, K.H., et al., Phys. Rev. Lett. **73** (1994) 436.
- [17] CHANG, C.S., et al., Phys. Plasmas **1** (1994) 3857.
- [18] JAEGER, E.F., et al., Nucl. Fusion **33** (1993) 179.
- [19] BUDNY, R.V., et al., Nucl. Fusion **32** (1992) 429.
- [20] VAN EESTER, D., Plasma Phys. Lab., École royale militaire/Koninklijke Militaire School, Brussels, personal communication, 1994.
- [21] BOIVIN, R.L., et al., Rev. Sci. Instrum. **63** (1992) 4418.
- [22] GOLDSTON, R.J., et al., Phys. Rev. Lett. **47** (1981) 647.
- [23] BOIVIN, R.L., et al., Nucl. Fusion **33** (1993) 449.
- [24] BOIVIN, R.L., et al., Rev. Sci. Instrum. **61** (1990) 3208.
- [25] TAYLOR, G., et al., Plasma Phys. Control. Fusion **36** (1994) 523.

(Manuscript received 5 September 1994

Final manuscript accepted 14 June 1995)